Supporting Information

Adaptable sublattice stabilized high-entropy materials with superior thermoelectric performance

Haotian Gao[a], Kunpeng Zhao[a,b], Hexige Wuliji[a*], Min Zhu[c], Beibei Xu[c], He Lin[d], Liting Fei[d], Hongyao Zhang[d], Zhengyang Zhou[e], Jingdan Lei[a], Heyang Chen[a], Shun Wan[b], Tian-Ran Wei[a,b], and Xun Shi[a,e*]*

A: Lattice thermal conductivity calculations

The lattice thermal conductivity is calculated by subtracting the carrier contribution κ_e and bipolar contribution $\kappa_{bipolar}$ from the total κ, i.e. $\kappa_L = \kappa - \kappa_e - \kappa_{bipolar}$, where κ_L is lattice thermal conductivity, κ is measured total thermal conductivity, κ_e is electrical thermal conductivity, and $\kappa_{bipolar}$ is bipolar thermal conductivity. The carrier thermal conductivity can be determined by the Wiedemann-Franz law: $\kappa_e=L_0\sigma T$, where T is absolute temperature, σ is experimental electrical conductivity and L is the Lorenz factor. The simple two-band model proposed by Simon[1], i.e. one parabolic conduction band and one parabolic valence band, is used to calculate the bipolar contribution $\kappa_{bipolar}$. The Lorenz factor L can be estimated by Equations S1−S2[1]:

$$S = \frac{k_B}{e}\left(\frac{(\lambda+2)F_{\lambda+1}(\eta)}{(\lambda+1)F_\lambda(\eta)} - \eta\right) \quad \text{(S1)}$$

$$L = \left(\frac{k_B}{e}\right)^2 \left\{\frac{(\lambda+3)F_{\lambda+2}(\eta)}{(\lambda+1)F_\lambda(\eta)} - \left[\frac{(\lambda+2)F_{\lambda+1}(\eta)}{(\lambda+1)F_\lambda(\eta)}\right]^2\right\} \quad \text{(S2)}$$

where e is elementary charge, k_B is Boltzmann constant, S is experimental Seebeck coefficient, η is reduced Fermi level, λ is scattering parameter, and $F_\lambda(\eta)$ is Fermi integrate defined as $F_\lambda(\eta) = \int_0^\infty \frac{x^\lambda}{1+e^{x-\eta}}dx$.

The room temperature reduced Fermi level is derived from both the carrier

concentration and Seebeck coefficient on the basis of single band approximation. Assuming that the intrinsic carrier n_0 is negligible and external doping is fully excitation, external dopant N_D is equal to be experimental carrier concentration at room temperature. Therefore, the electron concentration, hole concentration and reduced Fermi level can be solved by Equations S3−S5[1]:

$$n = p_0 + N_D \tag{S3}$$

$$n = 4\pi\left(\frac{2m_e^* k_B T}{h^2}\right)^{3/2} F_\lambda(\eta) \tag{S4}$$

$$p = 4\pi\left(\frac{2m_h^* k_B T}{h^2}\right)^{3/2} F_\lambda(-\eta - E_g) \tag{S5}$$

where m_e^* is electron effective mass, m_h^* is hole effective mass and E_g is band gap.

The electron Seebeck coefficient S_n and hole Seebeck coefficient S_p can be calculated by:

$$S_n = \pm\frac{k_B}{e}\left(\frac{(\lambda+2)F_{\lambda+1}(\eta)}{(\lambda+1)F_\lambda(\eta)} - \eta\right) \tag{S6}$$

$$S_p = \pm\frac{k_B}{e}\left(\frac{(\lambda+2)F_{\lambda+1}(-\eta - E_g)}{(\lambda+1)F_\lambda(-\eta - E_g)} + \eta + E_g\right) \tag{S7}$$

The electron conductivity σ_n and hole conductivity σ_p can be estimated by Equations S8−S10:

$$\sigma_n = n_0 \mu_{aver} e \tag{S8}$$

$$\sigma_h = A p_0 \mu_{aver} e \tag{S9}$$

$$\sigma_n S_n + \sigma_p S_p = \sigma S \tag{S10}$$

where μ_{aver} is average mobility, and A is a parameter to fit calculated Seebeck coefficient and measured Seebeck coefficient. Finally, bipolar thermal conductivity can be calculated by[1]:

$$\kappa_{bipolar} = \frac{\sigma_n \sigma_p}{\sigma_n + \sigma_p}\left(S_n - S_p\right)^2 T \tag{S11}$$

B: Calculation of the Mg content

It is assumed that each Bi_{Sn} introduces one electron and each V_{Mg} introduces two holes. Then, the content of Mg vacancies can be estimated by[2]:

$$x_V = \frac{1}{2}\left(x - \Delta n \frac{M}{\rho N_A} \right) \quad \text{(S12)}$$

$$\Delta n = n - n_0 \quad \text{(S13)}$$

where x_v is the content of V_{Mg}, x is the nominal Bi content, n is the measured carrier concentration for our $Mg_{2-\delta}Si_{0.12}Ge_{0.13}Sn_{0.75-x}Bi_x$ samples, n_0 is the carrier concentration of $Mg_2Si_{0.12}Ge_{0.13}Sn_{0.75}$, M is the relative molecular mass, ρ is the sample's density, and N_A is the Avogadro constant. Therefore, the content of Mg (x_{Mg}) is given by

$$x_{Mg} = 2 - x_V \quad \text{(S14)}$$

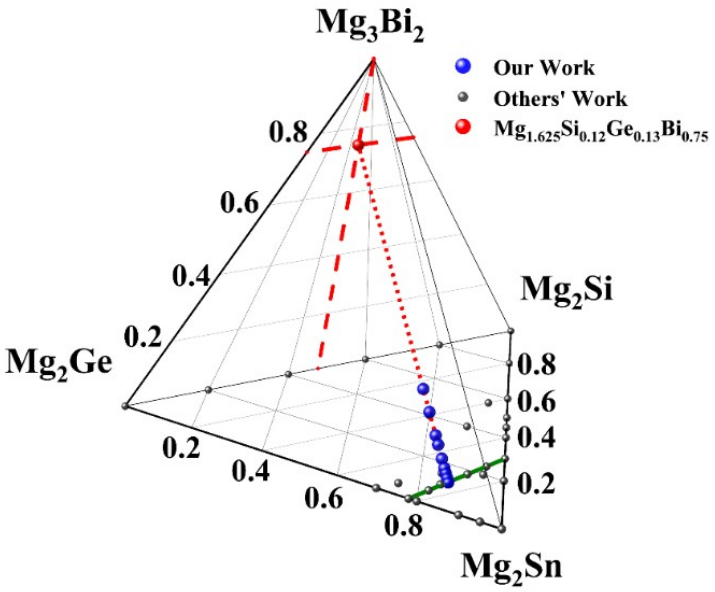

Fig. S1. Phase diagram of Mg_2Si-Mg_2Ge-Mg_2Sn-Mg_3Bi_2 quaternary system. The black sphere symbols represent the data from references[3-10], while the blue sphere symbols represent the samples synthesized in this work.

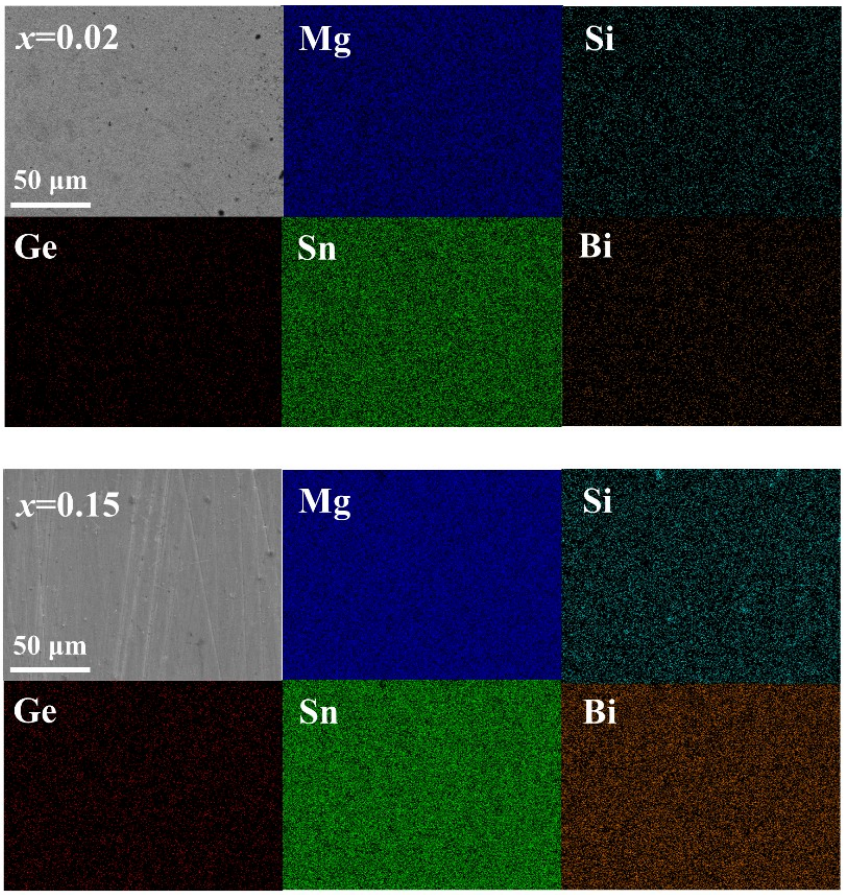

Fig. S2. Backscattered electron microscopy (BSE) images and corresponding elemental energy-dispersive X-ray spectroscopy (EDS) mapping of $Mg_{2-\delta}Si_{0.12}Ge_{0.13}Sn_{0.75-x}Bi_x$ (x = 0.02, 0.15)

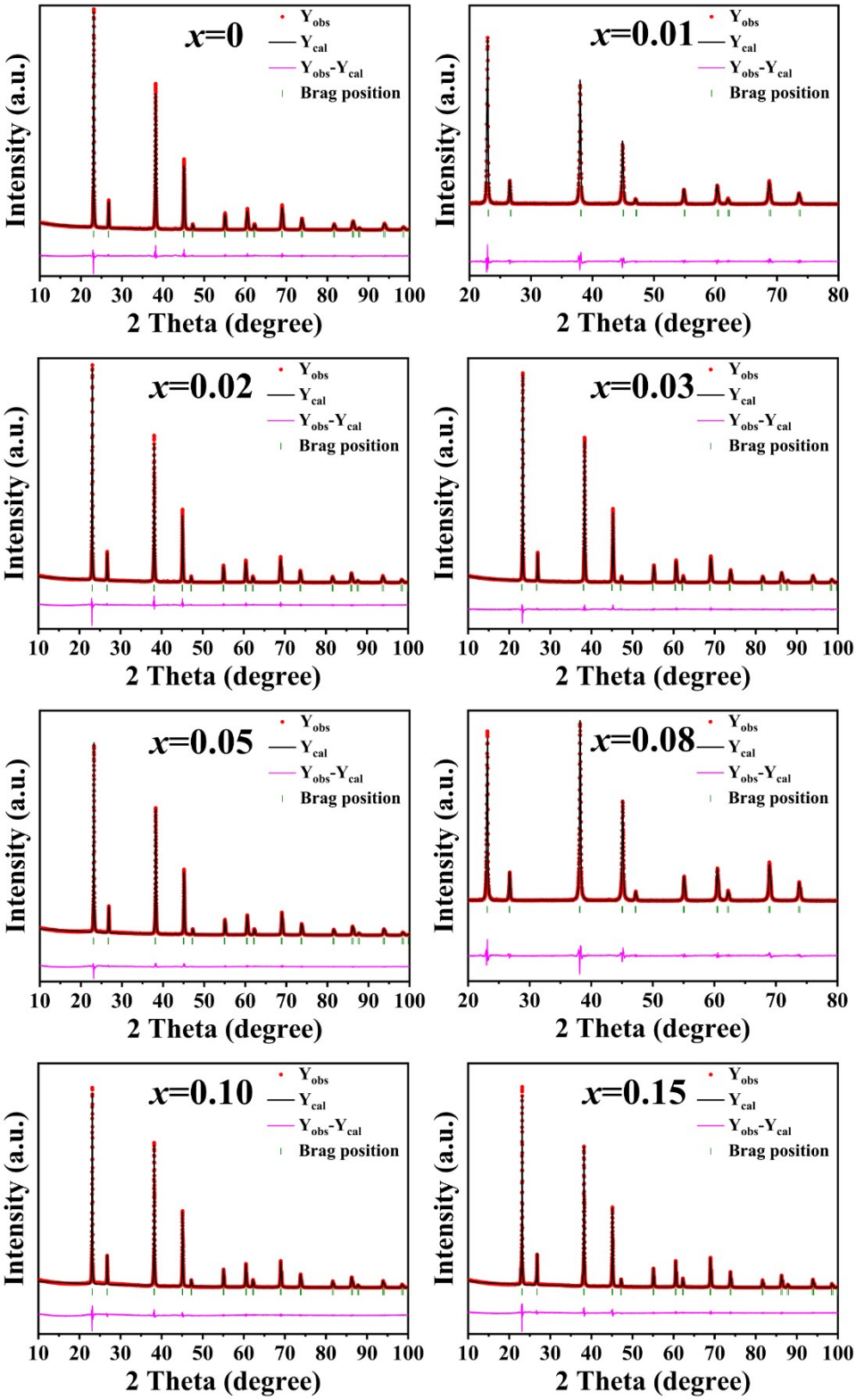

Fig. S3. Observed (red) and calculated (black) diffraction patterns and difference profiles (pink) for samples $Mg_{2-\delta}Si_{0.12}Ge_{0.13}Sn_{0.75-x}Bi_x$ (x=0, 0.01, 0.02, 0.03, 0.05, 0.08, 0.10, 0.15) at room temperature.

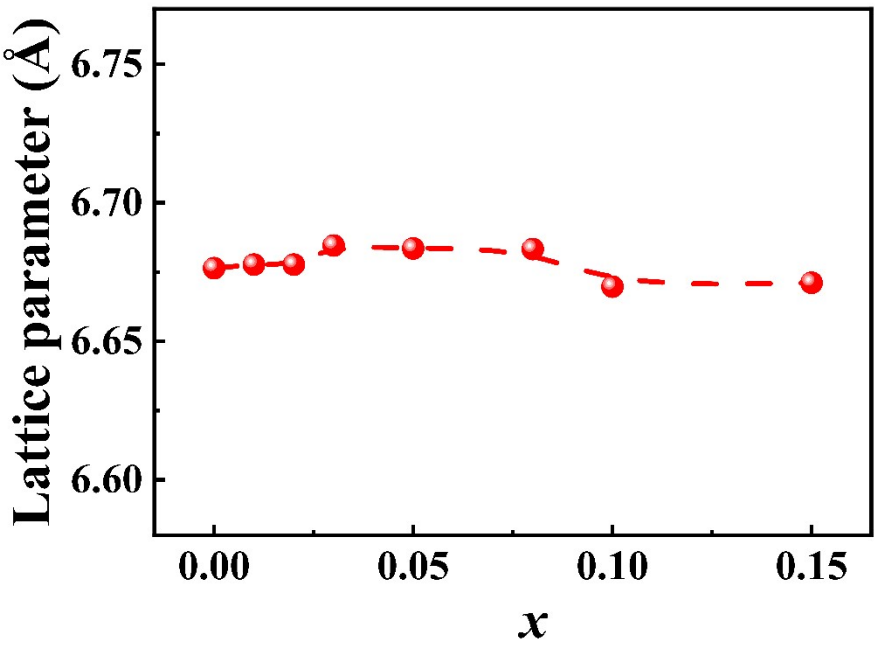

Fig. S4. Lattice parameter as a function of Bi content *x*.

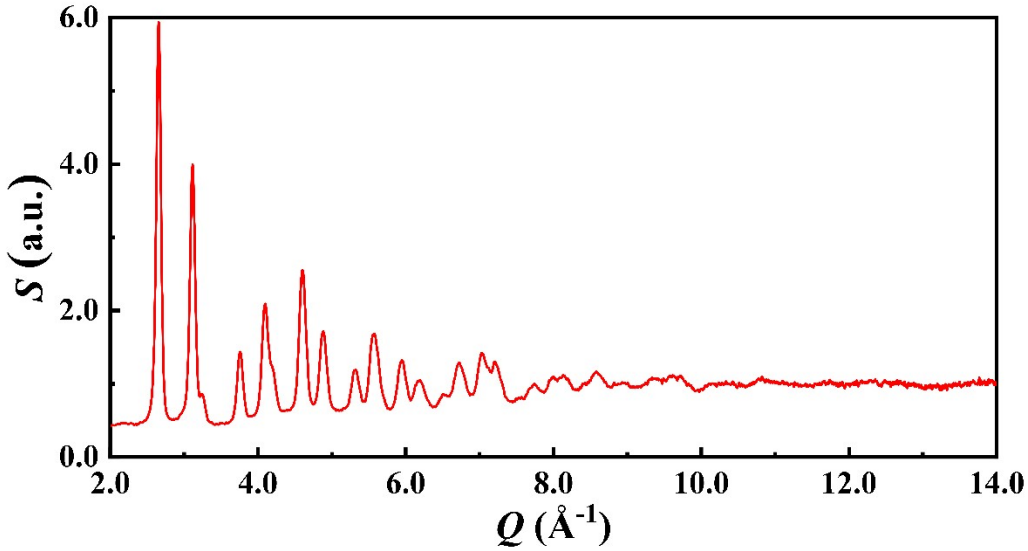

Fig. S5. Structure factor *S* as a function of *Q*.

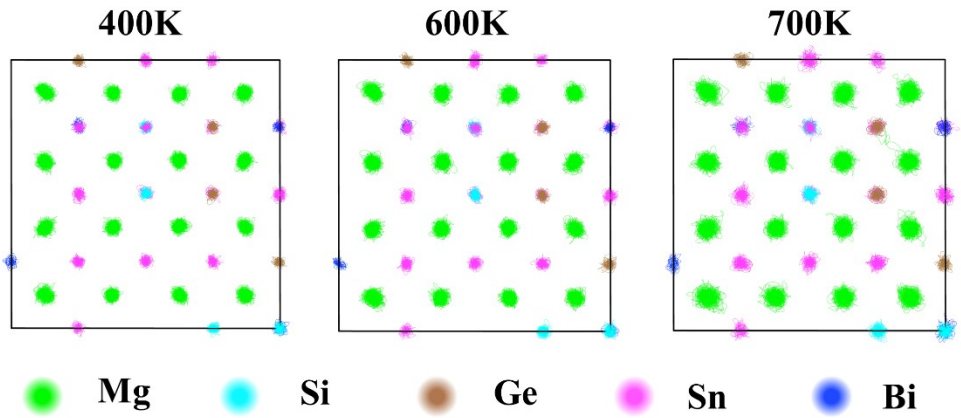

Fig. S6. Molecular dynamics simulations of the trajectory of Mg, Si, Ge, Sn, Bi at 400 K, 600 K, and 700 K

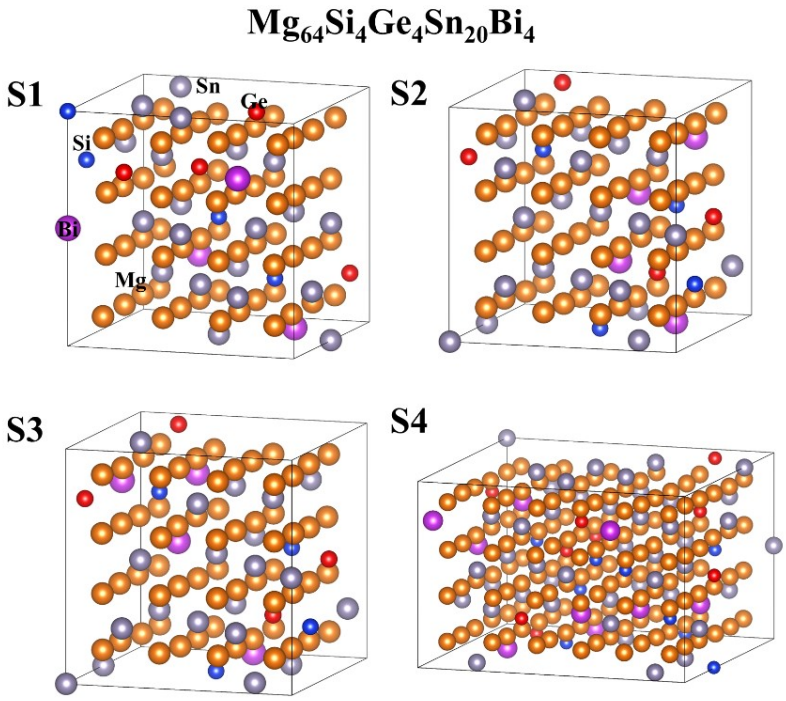

Fig. S7. Crystal structure of different supercells. (a) S1 (2×2×2 supercell), (b) S2 (2×2×2 supercell), (c) S3 (2×2×2 supercell), and (d) S4 (3×3×2 supercell).

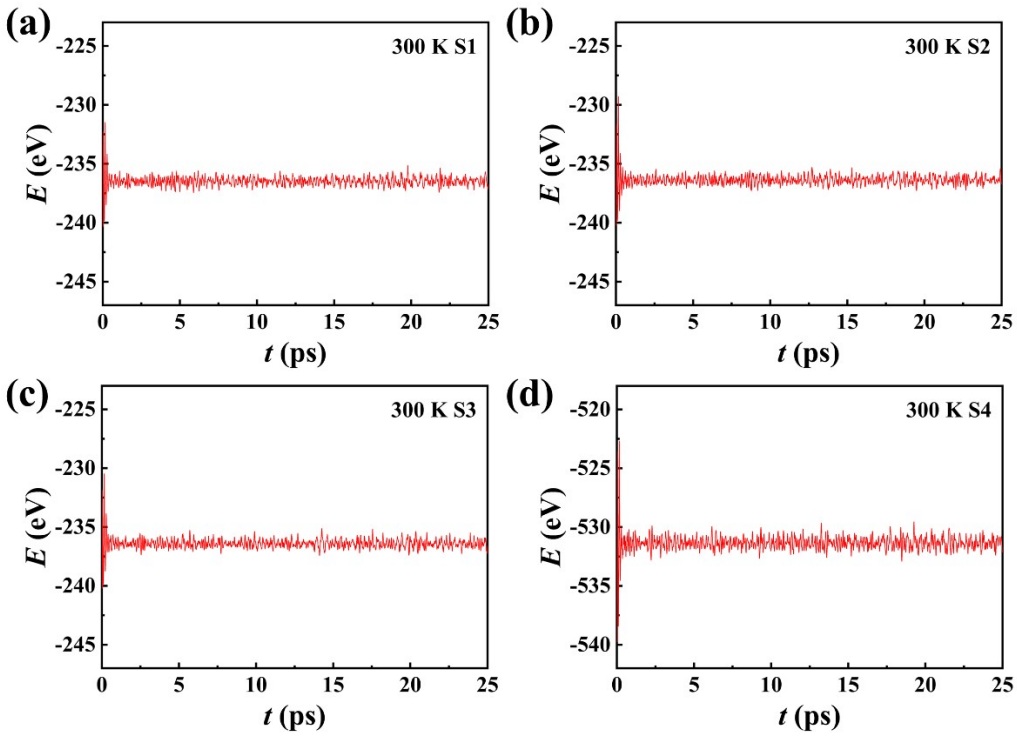

Fig. S8. Total energy *E* as a function of stimulation time *t* for different supercells. (a) S1 (2×2×2 supercell), (b) S2 (2×2×2 supercell), (c) S3 (2×2×2 supercell), and (d) S4 (3×3×2 supercell).

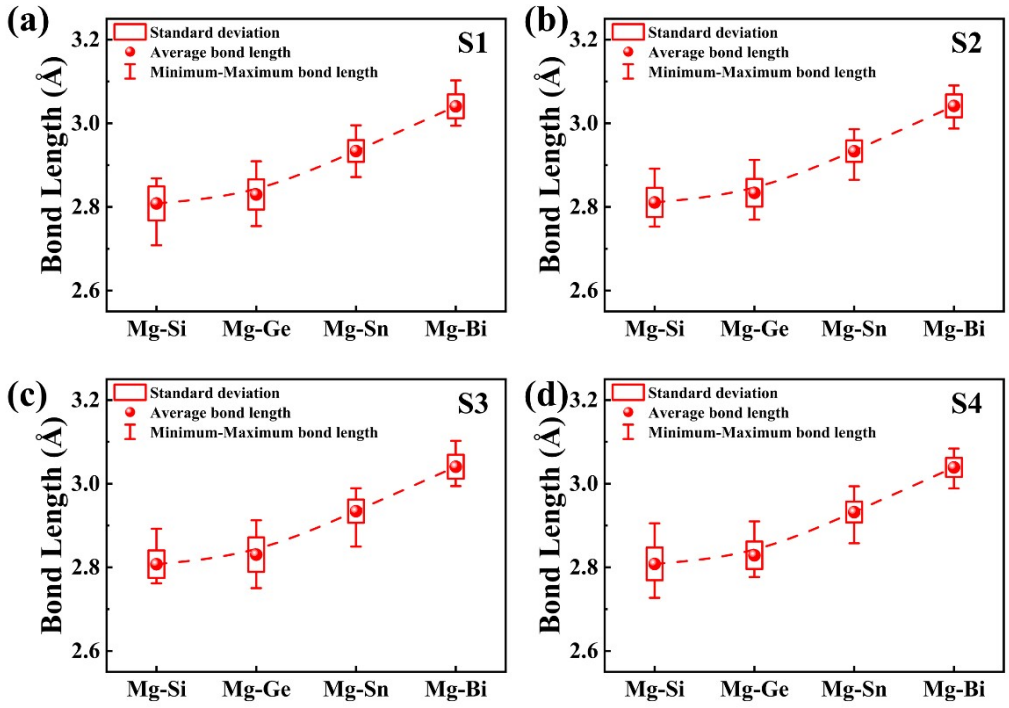

Fig. S9. Calculated bond length for different supercells. (a) S1 (2×2×2 supercell), (b) S2 (2×2×2 supercell), (c) S3 (2×2×2 supercell), and (d) S4 (3×3×2 supercell).

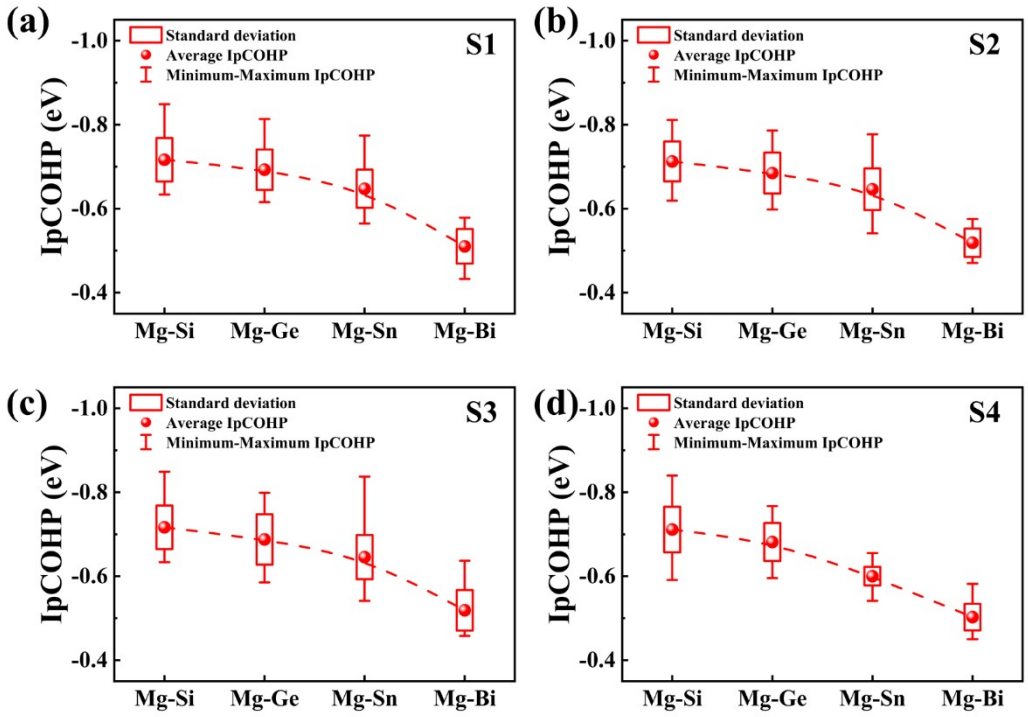

Fig. S10. Calculated IpCOHP for different supercells. (a) S1 (2×2×2 supercell), (b) S2 (2×2×2 supercell), (c) S3 (2×2×2 supercell), and (d) S4 (3×3×2 supercell).

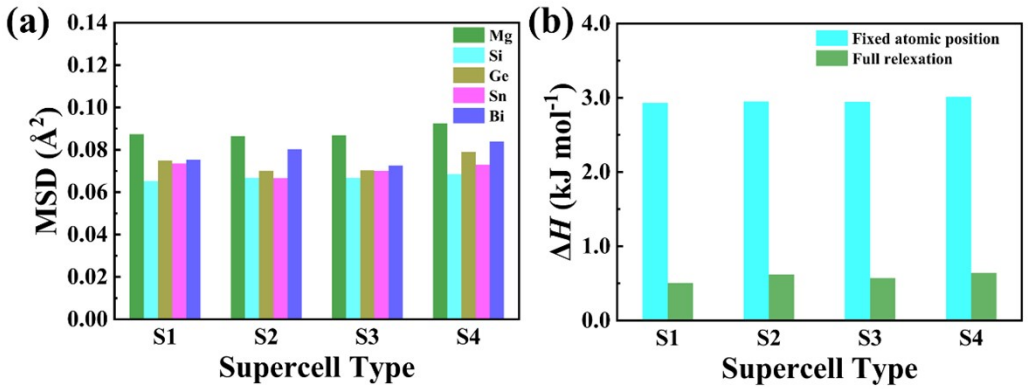

Fig. S11. Calculated (a) MSD at 300 K and (b) mixing enthalpy ΔH for different supercells.

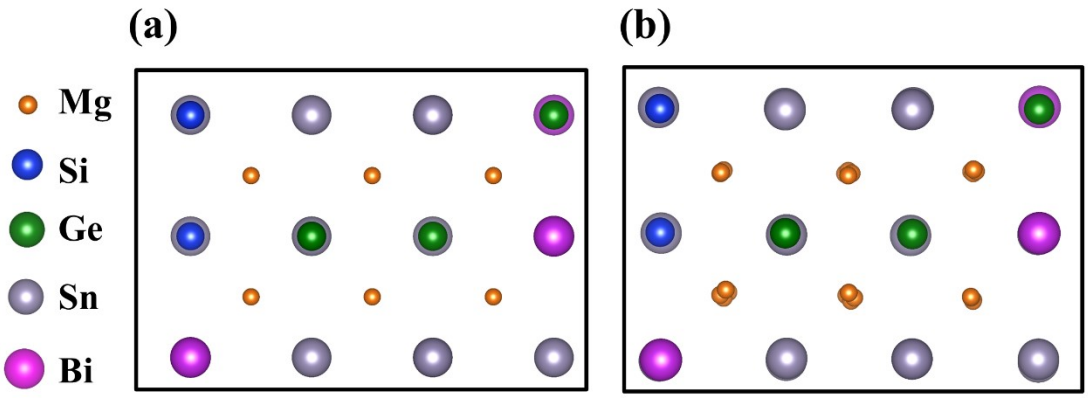

Fig. S12. The obtained crystal structures of $Mg_2Si_4Ge_4Sn_{20}Bi_4$: (a) volume relaxation with fixed atomic positions within the cubic lattice, (b) full relaxation with the cell volume, shape and atomic positions optimized.

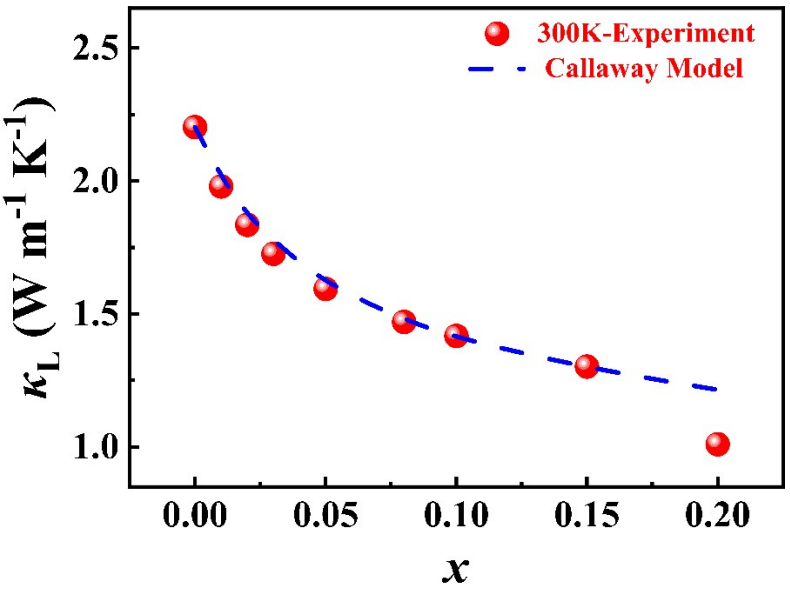

Fig. S13. Lattice thermal conductivity κ_L at 300 K as a function of Bi content x. The dashed line denotes the calculated κ_L by the Callaway model.

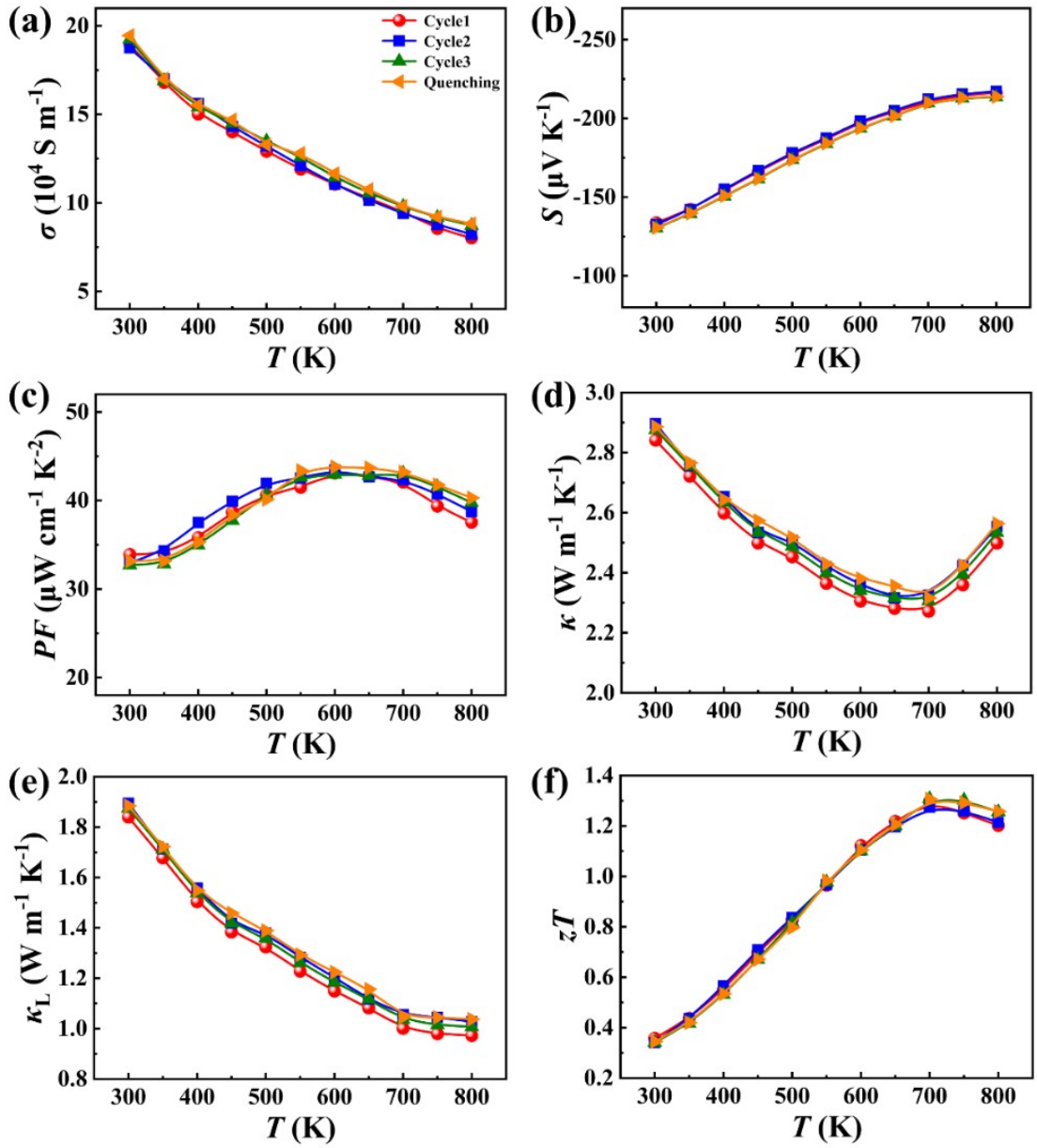

Fig. S14. Temperature dependence of (a) electrical conductivity σ, (b) Seebeck coefficient S, (c) power factor PF, (d) thermal conductivity κ, (e)lattice thermal conductivity κ_L and (d) zT of sample $Mg_{2-\delta}Si_{0.12}Ge_{0.13}Sn_{0.73}Bi_{0.02}$ after three cycles and after quenching at 800 K.

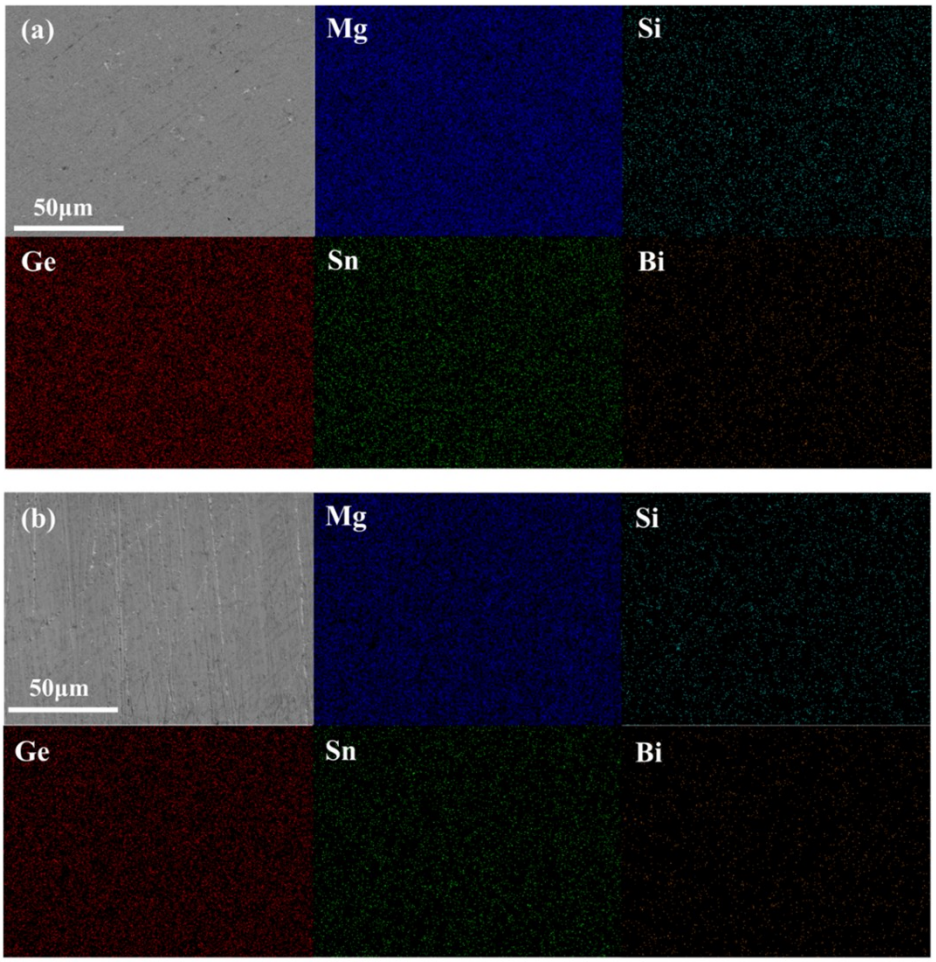

Fig. S15. Backscattered electron microscopy (BSE) images and corresponding elemental energy-dispersive X-ray spectroscopy (EDS) mapping of $Mg_{2-\delta}Si_{0.12}Ge_{0.13}Sn_{0.73}Bi_{0.02}$. (a) after three cycles; (b) after quenching.

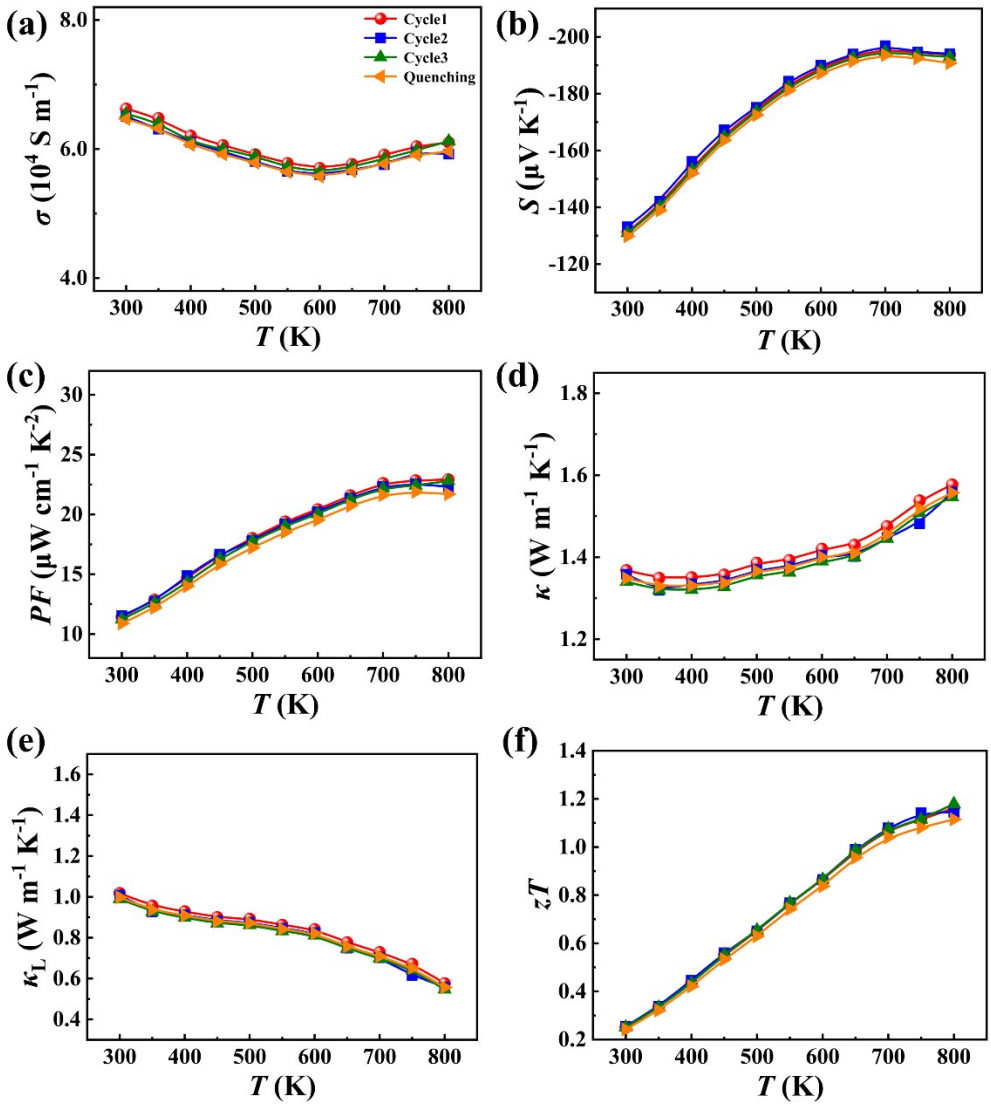

Fig. S16. Temperature dependence of (a) electrical conductivity σ, (b) Seebeck coefficient S, (c) power factor PF, (d) thermal conductivity κ, (e)lattice thermal conductivity κ_L and (d) zT of sample $Mg_{2-\delta}Si_{0.12}Ge_{0.13}Sn_{0.55}Bi_{0.20}$ after three cycles and after quenching at 800 K.

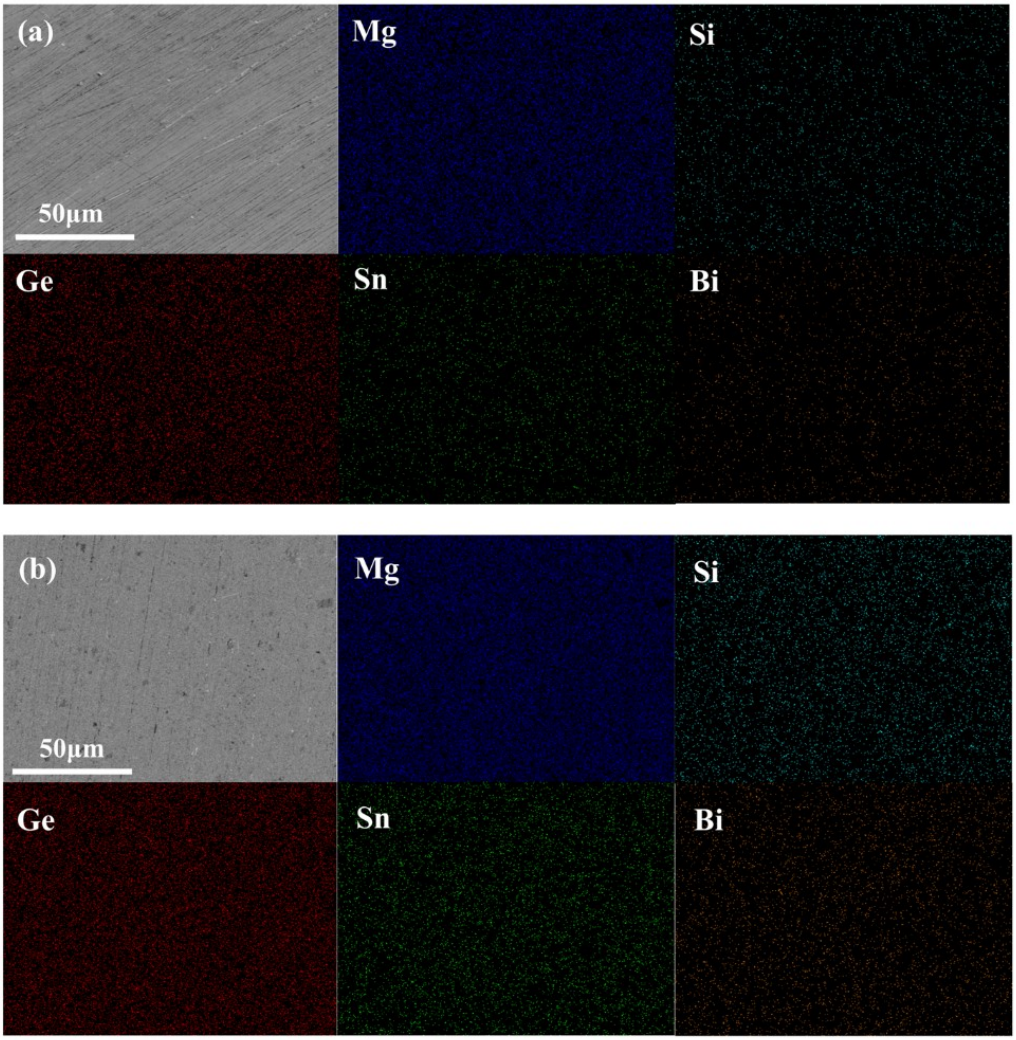

Fig. S17. Backscattered electron microscopy (BSE) images and corresponding elemental energy-dispersive X-ray spectroscopy (EDS) mapping of $Mg_{2-\delta}Si_{0.12}Ge_{0.13}Sn_{0.55}Bi_{0.20}$ (a) after three cycles; (b) after quenching.

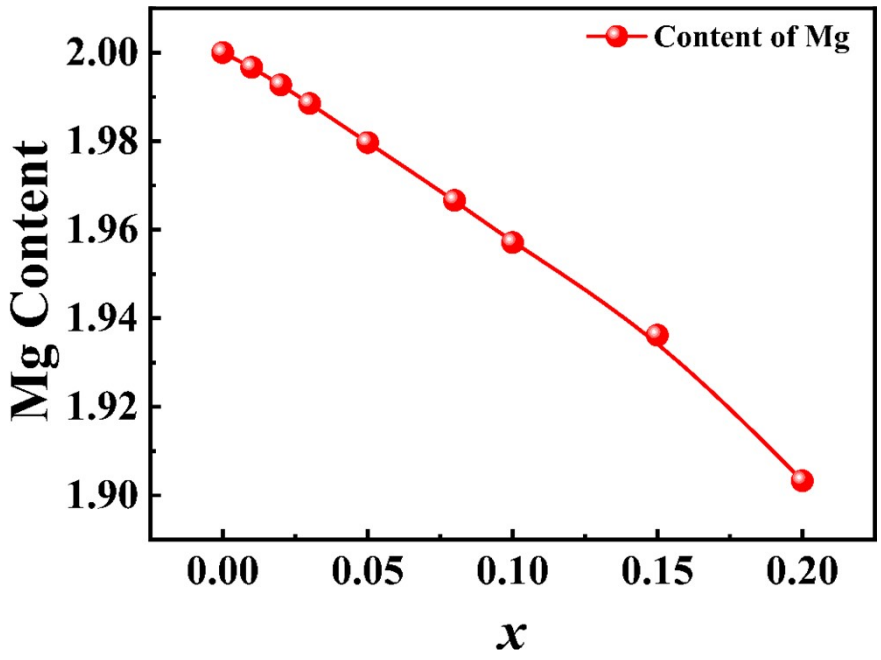

Fig. S18. Calculated Mg content as a function of Bi content *x*

Table S1. Atomic radius, electronegativity, and the most likely valence state of Mg, Si, Ge, Sn and Bi in $Mg_{2-\delta}Si_{0.12}Ge_{0.132}Sn_{0.748-x}Bi_x$.

Atom	Atomic radius (Å)	Electronegativity	Valence state
Mg	1.50	1.31	+2
Si	1.10	1.90	-4
Ge	1.25	2.01	-4
Sn	1.45	1.96	-4
Bi	1.60	2.02	-3

Table S2. Rietveld refined results of samples $Mg_{2-\delta}Si_{0.12}Ge_{0.13}Sn_{0.75-x}Bi_x$

Composition	Atom	x	y	z	Occ.	U_{iso}	Site	Sym.
***x*=0**	Mg	0.25	0.75	0.75	0.994	0.014	8c	-43m
	Si	0	0	0	0.120	0.006	4a	m-3m
	Ge	0	0	0	0.130	0.006	4a	m-3m
	Sn	0	0	0	0.750	0.006	4a	m-3m
***x*=0.01**	Mg	0.25	0.75	0.75	1.000	0.011	8c	-43m
	Si	0	0	0	0.120	0.002	4a	m-3m
	Ge	0	0	0	0.130	0.002	4a	m-3m
	Sn	0	0	0	0.740	0.002	4a	m-3m
	Bi	0	0	0	0.010	0.002	4a	m-3m
***x*=0.02**	Mg	0.25	0.75	0.75	0.981	0.014	8c	-43m
	Si	0	0	0	0.120	0.006	4a	m-3m
	Ge	0	0	0	0.130	0.006	4a	m-3m
	Sn	0	0	0	0.730	0.006	4a	m-3m
	Bi	0	0	0	0.020	0.006	4a	m-3m
***x*=0.03**	Mg	0.25	0.75	0.75	0.983	0.014	8c	-43m
	Si	0	0	0	0.120	0.005	4a	m-3m
	Ge	0	0	0	0.130	0.005	4a	m-3m
	Sn	0	0	0	0.720	0.005	4a	m-3m
	Bi	0	0	0	0.030	0.005	4a	m-3m
***x*=0.05**	Mg	0.25	0.75	0.75	0.973	0.014	8c	-43m
	Si	0	0	0	0.120	0.005	4a	m-3m

	Ge	0	0	0	0.130	0.005	4a	m-3m
	Sn	0	0	0	0.700	0.005	4a	m-3m
	Bi	0	0	0	0.050	0.005	4a	m-3m
	Mg	0.25	0.75	0.75	1.000	0.016	8c	-43m
	Si	0	0	0	0.120	0.007	4a	m-3m
***x*=0.08**	Ge	0	0	0	0.130	0.007	4a	m-3m
	Sn	0	0	0	0.670	0.007	4a	m-3m
	Bi	0	0	0	0.080	0.007	4a	m-3m
	Mg	0.25	0.75	0.75	0.961	0.020	8c	-43m
	Si	0	0	0	0.120	0.014	4a	m-3m
***x*=0.10**	Ge	0	0	0	0.130	0.014	4a	m-3m
	Sn	0	0	0	0.650	0.014	4a	m-3m
	Bi	0	0	0	0.100	0.014	4a	m-3m
	Mg	0.25	0.75	0.75	0.956	0.024	8c	-43m
	Si	0	0	0	0.120	0.017	4a	m-3m
***x*=0.15**	Ge	0	0	0	0.130	0.017	4a	m-3m
	Sn	0	0	0	0.600	0.017	4a	m-3m
	Bi	0	0	0	0.150	0.017	4a	m-3m
	Mg	0.25	0.75	0.75	1.000	0.021	8c	-43m
	Si	0	0	0	0.120	0.009	4a	m-3m
***x*=0.20**	Ge	0	0	0	0.130	0.009	4a	m-3m
	Sn	0	0	0	0.550	0.009	4a	m-3m

Bi	0	0	0	0.200	0.009	4a	m-3m

Table S3. Quality factor of Rietveld refinement.

Composition	R_p	wR_p	R_{obs}	wR_{obs}	R_{all}	wR_{all}
***x*=0**	4.63%	6.30%	1.51%	2.40%	1.51%	2.40%
***x*=0.01**	5.04%	6.93%	1.52%	2.01%	1.52%	2.01%
***x*=0.02**	5.09%	6.58%	1.49%	2.24%	1.49%	2.24%
***x*=0.03**	3.64%	5.17%	1.20%	1.87%	1.20%	1.87%
***x*=0.05**	5.10%	6.45%	1.45%	2.23%	1.45%	2.23%
***x*=0.08**	4.16%	5.98%	1.19%	1.82%	1.19%	1.82%
***x*=0.10**	6.97%	8.78%	1.29%	2.53%	1.29%	2.53%
***x*=0.15**	6.13%	7.75%	1.11%	2.15%	1.11%	2.15%
***x*=0.20**	5.26%	7.26%	1.33%	2.24%	1.33%	2.24%

Table S4. ADP and error of samples $Mg_{2-\delta}Si_{0.12}Ge_{0.13}Sn_{0.75-x}Bi_x$.

Composition	Mg U_{iso} (Å^2)	Error (Å^2)	X U_{iso} (Å^2)	Error (Å^2)
***x*=0**	0.0144	4×10^{-4}	0.006	1.2×10^{-4}
***x*=0.01**	0.015	4×10^{-4}	0.007	1.2×10^{-4}
***x*=0.02**	0.0138	4×10^{-4}	0.00634	1.3×10^{-4}

***x*=0.03**	0.014	3×10^{-4}	0.00541	9×10^{-5}
***x*=0.05**	0.0138	4×10^{-4}	0.00526	1.4×10^{-4}
***x*=0.08**	0.016	2×10^{-4}	0.0073	1×10^{-4}
***x*=0.10**	0.0202	9×10^{-4}	0.0137	8×10^{-4}
***x*=0.15**	0.0236	7×10^{-4}	0.0168	6×10^{-4}

Table S5. PDF fits results of samples $Mg_{2-\delta}Si_{0.12}Ge_{0.13}Sn_{0.65}Bi_{0.10}$.

Structure	Atom	x	y	z	Occ.	U_{iso}	Site	Sym.
Broken symmetry model	Mg1	0.234	0.766	0.766	0.960	3.520	1a	1
	Mg2	0.765	0.234	0.766	0.960	3.520	1a	1
	Mg3	0.765	0.766	0.234	0.960	3.520	1a	1
	Mg4	0.234	0.234	0.234	0.960	3.520	1a	1
	Mg5	0.765	0.234	0.234	0.960	3.520	1a	1
	Mg6	0.234	0.766	0.234	0.960	3.520	1a	1
	Mg7	0.765	0.766	0.766	0.960	3.520	1a	1
	Mg8	0.234	0.234	0.766	0.960	3.520	1a	1
	Si	0	0	0	0.120	2.180	4a	m-3m
	Ge	0	0	0	0.130	2.180	4a	m-3m
	Sn	0	0	0	0.650	2.180	4a	m-3m
	Bi	0	0	0	0.100	2.180	4a	m-3m
	Mg	0.25	0.75	0.75	0.961	0.045	8c	-43m

	Si	0	0	0	0.120	0.021	4a	m-3m
	Ge	0	0	0	0.130	0.021	4a	m-3m
	Sn	0	0	0	0.650	0.021	4a	m-3m
	Bi	0	0	0	0.100	0.021	4a	m-3m

Table S6. The atomic radius, ionic radius, and orbital energy of Mg, Si, Ge, Sn and Bi.

Elements	Atomic radius (Å)	Ionic radius (Å)	Orbital energy
Mg	1.50	0.86	-7.65 eV (s orbital)
Si	1.10	0.54	-7.78 eV (p orbital)
Ge	1.25	0.67	-7.54 eV (p orbital)
Sn	1.45	0.83	-7.01 eV (p orbital)
Bi	1.60	1.17	-8.15 eV (p orbital)

Reference

1. R. Simon, *J. Appl. Phys.*, 1962, **33**, 1830-1841.
2. J. Lei, H. Wuliji, K. Zhao, T.-R. Wei, Q. Xu, P. Li, P. Qiu and X. Shi, *J. Mater. Chem. A*, 2021, **9**, 25944-25953.
3. J. de Boor, U. Saparamadu, J. Mao, K. Dahal, E. Müller and Z. Ren, *Acta Mater.*, 2016, **120**, 273-280.
4. A. U. Khan, N. V. Vlachos, E. Hatzikraniotis, G. S. Polymeris, C. B. Lioutas, E. C. Stefanaki, K. M. Paraskevopoulos, I. Giapintzakis and T. Kyratsi, *Acta Mater.*, 2014, **77**, 43-53.
5. H. Ihou-Mouko, C. Mercier, J. Tobola, G. Pont and H. Scherrer, *J. Alloys Compd.*, 2011, **509**, 6503-6508.
6. R. J. LaBotz, D. R. Mason and D. F. O'Kane, *J. Electrochem. Soc.*, 1963, **110**, 127.
7. W. Liu, X. Tan, K. Yin, H. Liu, X. Tang, J. Shi, Q. Zhang and C. Uher, *Phys. Rev. Lett.*, 2012, **108**, 166601.
8. W. Liu, H. S. Kim, S. Chen, Q. Jie, B. Lv, M. Yao, Z. Ren, C. P. Opeil, S. Wilson, C.-W. Chu and Z. Ren, *Proc. Natl. Acad. Sci. USA*, 2015, **112**, 3269-3274.
9. A. U. Khan, N. Vlachos and T. Kyratsi, *Scripta Mater.*, 2013, **69**, 606-609.

10. W. Liu, J. Zhou, Q. Jie, Y. Li, H. S. Kim, J. Bao, G. Chen and Z. Ren, *Energy Environ. Sci.*, 2016, **9**, 530-539.